High-efficient biosorbent of Pb2+ derived from the organic frameworks of Cladophora rupestris

Lu-sheng Zhang
Anhui Agricultural University
Xiao-yu Feng
Anhui Agricultural University
Ling-sheng Li
Anhui Agricultural University
Yu Sun
Anhui Agricultural University
Xin-yi Tao
Anhui Agricultural University
Qian Yin
Anhui Agricultural University
Xin-yue Li
Anhui Agricultural University
Shi-ying Ma
Anhui Agricultural University
deju Cao (cdj@ahau.edu.cn)
Anhui Agricultural University https://orcid.org/0000-0003-0911-0006
Zhao-wen Liu
Chizhou University

Research Article

Keywords: Cladophora rupestris organic frameworks, Pb2+, isotherm adsorption models, SEM–EDS, FTIR, XPS

Posted Date: April 11th, 2023

DOI: https://doi.org/10.21203/rs.3.rs-2485829/v1

Abstract

This study aims to investigate the Pb^{2+} adsorption performance of the organic frameworks derived from *Cladophora rupestris* (CROF). The characterizations of CROF and Pb^{2+} adsorption process was analysed using SEM-EDS, LPSA, BET, PH_{PZC}, FTIR and XPS. The results was showed that CROF was porous structure, had both macroporous and microporous properties. The particle size is normally distributed with a median diameter of 36.8 μm. PH_{PZC} of CROF was 7.02. The CROF adsorption isotherms and kinetics closely matched Langmuir model and Pseudo-second-order(PSO), respectively, the adsorption behaviors can be classified as monolayer chemical adsorption. The maximum adsorption capacity (Qm) was 15.02 mg/g and 97% of the Pb^{2+} was adsorbed onto the CROF within 20 min. And the adsorption was exothermic, spontaneous and minimised randomness. Additionally, the biosorbent has outstanding Pb^{2+}adsorption capability due to pore filling, ion exchange, Pb-πinteraction, and surface complexation between nitrogen and oxygen functional groups(OFGs and NFGs). CROF is economical and environmentally friendly and it can be used as an adsorbent to take Pb^{2+} out from waterbodies.

Highlights

- The CROF adsorption isotherms and kinetics closely matched Langmuir model and PSO.
- Maximum capacity(Qm) of CROF was 15.02 mg/g.
- 97 % of the Pb^{2+} was adsorbed onto the CROF within 20 min.
- The form of Pb in CROF was Pb^{2+} and Pb combined with OFGs ,have some the the π-π bindings of Pb^{2+} and O in NFGs.

Introduction

Heavy metals (HMs) is one of the inorganic pollutants prevalent in water (Fang et al. 2022).Pb^{2+} is the most significant HMs pollutants and comes from a variety of sources, including gasoline emission, mining, automobile exhaust, etc.(Yang et al. 2022), due to microbial or chemical behavior cannot degrade it (Wang et al. 2022d),threatening the human health and environment greatly(Ling et al. 2017).Therefore, rapid and efficient decontamination Pb^{2+} is crucial to environmental remediation.

Biochars and Various modified biochars were used to clean up HMs contamination widely (Wang et al. 2015), such as biochar derived from oil tea camellia shell modifed by silicate for Cd^{2+} removal(Cai et al. 2021), biochar adsorb Pb^{2+} and at the same time enhance through dissolved organic matter(Wang et al. 2022d),and humic-like and protein-like compounds contributed to Pb^{2+} sorption(Zhang et al. 2017). The Qm of Pb^{2+} on fresh biochar were 279.85 and 286.07 $mg{\cdot}g^{-1}$ at 350°C and 650°C (Wang et al. 2019). But the preparation cost of biochar is relatively high, and limits the development of technology.The inorganic and organic frameworks of biological materials play an important role in HMs absorption, Li et al. (2021a)demonstrated metal-organic frameworks could adsorb UO_2^{2+} and ReO_4^- in water with remarkable efficiency. Silicon dioxide(SiO_2)decorated with nano-ferrous oxalate for Pb^{2+} removal(Zeng et al. 2020), Jayakumar et al. (2022) studied the ability of brown algae *Sargassum polycystum* could adsorb Cd^{2+} and Zn^{2+} and found that the Qm of Cd^{2+} and Zn^{2+} were 105.3mg/g and 116.2 mg/g ,respectively. Meanwhile, the adsorption of Pb^{2+} on the fractured structure of microplastics was

studied by Jiang et al. (2022). *Cladophora rupestris* was widely distributed in water environment, is a kind of renewable biological resources, it often grows out of management and spreads quickly (Sucaldito &Camacho 2017). Green algae may be used as a source material for absorbing HMs because biomass waste have a porous structure(Sucaldito &Camacho 2017). *C. rupestris* can accumulate $Pb^{2+}$and Cd^{2+}(Cao et al. 2015;Zhang et al. 2019),*Cladophora* is an noteworthy source of extremely crystalline cellulose material(Sucaldito &Camacho 2017), and high-efficient sorption of $Pb^{2+}$and Cd^{2+}. So it could be applied to absorbed HMs. In addition, the organic frameworks of *C. rupestris* was a relatively simple, economical, and can tolerate moderately polluted environment.

The primary purpose is to investigate the adsorption between Pb^{2+} and CROF in this paper. The characterizations of CROF and Pb^{2+} adsorption mechanisms was analysed using SEM-EDS, LPSA, BET, PH_{PZC} FTIR and XPS, Batch tests of adsorption kinetics, isotherm and thermodynamic were performed to evaluated Pb^{2+} Adsorption behaviours, which aims to provide a new and cost-effective algal biosorbent with performance of HMs removal in wastewater.

1. Experimental And Methods

1.1 Preparation of CROF

The samples of *C. rupestris* was collected from a pond water of Hefei in Anhui Province, China(32°30' N, 116°17'E), these raw materials were rinsed with running water repeatedly to remove dirt particles and impurities, later by ultrapure water several times, dried in an oven(80°C,12 h) to constant weight, and then the dried *C. rupestris* was crushed into powder to obtain particle size of 100 mesh by screening, CROF was saved in a brown bottle for standby application.

1.2 Batch adsorption experiments and Pb^{2+} content analysis

1.599 g $Pb(NO_3)_2$ dissolve in 1000 mL ultrapure water, stock solution of Pb^{2+}(1000 mg/L)was obtained with 0.01 mol/L $NaNO_3$ as the background electrolyte. 0.100 g of CROF and 25 mL of Pb^{2+} solutions were shaking at a rate of 180 rpm, then centrifuged at 10000 rpm, the supernatants were filtering by a 0.45 μm filter and analysis Pb^{2+} concetrations. Pb^{2+} concentrations were measured by a flame atomic absorption spectrometer(FAAS, ZEEnit 700P,GER Analytic Jena) with the absorbance at a wavelength of 283.3 nm.

1.3 Characterizations and combined forms analysis

The solide mixtures were lyophilized by Freeze Dryer(FD,SIM-4,USA).

1.3.1 SEM–EDS determination

A field emission Scanning Electron Microscope (SEM; S-4800, Hitachi, Japan) was used to look into micromorphology of CROF samples both prior to and after Pb^{2+} adsorption. Energy Dispersive X-ray Spectroscopy (EDS; X-MAXN 150, OXFORD, UK) equipped with SEM was used simultaneously to quantify the composition of elements on CROF surface(Yang et al. 2022).

1.3.2 PSD and BET analysis

A laser particle size analyzer(LPSA; BT-9300H Danton) was employed to assess the the pore size distribution(PSD) of CROF,the N2 adsorption/desorption isotherms was used to analyze pore structures of CROF with the method of Brunauer-Emmett-Teller(BET; Micromeritics ASAP 2460 USA) (Chen et al. 2021b;Esakkimuthu et al. 2022).

1.3.3 pHpzc analysis

0.100 g samples were taken into the volume of 25 mL in 0.01 mol/L $NaNO_3$ solutions with starting pH 2–9(Ahmad et al. 2019). Under the condition of 180 rpm, at 25 ℃, the suspensions reached equilibrium for 48 hours, then the final pH was assayed. When the initial pH = final pH(△pH = 0), the pH value is Point of zero charges (pHpzc).

1.3.4 FTIR analysis

0.001 g dried CROF treated with Pb^{2+} concentrations were 0, 5.0 and 50 mg/L were ground in an agate mortar with 0.100 g KBr and then compressed and molded into a small disk for the Fourier transform infrared spectroscopy analysis (FTIR; Nicolette is 50, Thermo Scientific, USA). Spectra were captured with a resolution of 2 cm^{-1} and wavenumbers of 4000 to 400 cm^{-1}(Chen et al. 2021a).

1.3.5 XPS analysis

The combined form of the elements(C, O and N) of the dried CROF treated with Pb^{2+} (0, 5.0 mg/L, 50 mg/L) were determined by X-ray photoelectron spectroscopy (XPS; Escalab 250, Thermo-VG Scientific, USA) with a monochromatized Al Ka (hv = 1486.6 eV) excitation source and a pass energy of 30 eV. Binding energies with the C 1s peak of the carbon contaminant at 284.80 eV were calibrated (Chen et al. 2021a; Liang et al. 2020).

1.4 Data Analysis

1.4.1 Determining the adsorption capacity and the removal percentage

The adsorption capacity and the removal percentage of Pb^{2+} on CROF could be calculated by the method of Chen et al. (2021b) and Xu et al. (2021).

1.4.2 adsorption kinetic models

The adsorption kinetics was studied by at constant temperature (25℃) and shook at 180 rpm with regular time intervals which were set as 1,3,5, 10 25,20, 25, 30, 35, 40, 45, 50, 55, 60 min .The results for adsorption capacity can be fitted by three adsorption kinetic models: Pseudo-first-order (PFO)(Eq. (1)), Pseudo-second-order(PSO) (Eq. (2)), and Elovich models(Eq. (3))(Xu et al. 2021):

$$q_t = q_e(1 - e^{-K_1 t})$$

1

$$q_t = K_2 q_e^2 t / (1 + K_2 q_e t)$$

2

$$q_t = \left(\frac{1}{\beta}\right) In[1 + (\alpha\beta t)]$$

3

where K_1, K_2 $and \beta$are constant of three adsorption kinetic models.

1.4.3 Isotherm adsorption models

The isotherm adsorption models were examined at a series of initial concentrations including 0, 5, 25, 30, 35, 40, 45, 50 mg/L and was shaken at 180 rpm and 30 ℃ for 24 h. The Langmuir model(Eq. (4)), Freundlich model(Eq. (5)) and Sips model (Eq. (6))were adopted to simulated the capture process of Pb^{2+}(Chen et al. 2021b; Wang et al. 2022c):

$$q_e = \frac{q_{max} K_L C_e}{1 + K_L C_e} (4)$$

$$q_e = K_f C e^{\frac{1}{n}} (5)$$

$$q_e = \frac{K_{LF} C_e^n}{1 + \partial_{LF} C_e^n} (6)$$

$$R_L = \frac{1}{1 + K_L C_0} (7)$$

where K_L $and K_f$ are the Langmuir and Freundlich constant, respectively, n is the Freundlich dimensionless exponent related to how favourable of the adsorption process. And the Langmuir parameter R_L(Eq. (7)) is also used to further investigate the viability of the adsorption (Zhang et al. 2022).

1.4.4 Adsorption thermodynamic models

The adsorption thermodynamic models were performed at 293, 298, 303 and 308 K. ΔH^θ, ΔS^θ and ΔG^θ were evaluated by the Van't Hoff(Eq. (8) and(Eq. (9))) and Gibbs free energy(Eq. (10)) formulas(Rahim et al. 2020;Zhang et al. 2022):

$$K_T = \frac{q_e}{c_e}$$

8

$$In\,(K_T) = -\left(\frac{\Delta H^\theta}{RT}\right) + \left(\frac{\Delta S^\theta}{R}\right)$$

9

$$\Delta G^\theta = -\mathrm{RT}\ln K_T$$

10

where, $K_T \mathrm{and} \mathrm{R}$ is the constant. The values of ΔH^θ and ΔS^θ is calculated from the slope and intercept t by the linear relationship between ln(qe/ce) and 1/T.

1.4.5 Statistic analysis

The relative errors were all less than 5% and every experiment was done in triplicate. OMNIC and Avantage were used for spectral processing. Origin 2018 was used to map the fitted data and facilitate simulations of adsorption kinetic, isotherm adsorption and adsorption thermodynamic models.

2. Results And Discussion

2.1 Characterizations of CROF

The SEM images, PSD, BET, PH_{PZC} of CROF were showed in Fig. 1, CROF has fibrous sheet structure with denser cracks and blocks (Fig. 1a). Figure 1b showed that the surface of porous on CROF was covered with fine particles, which could increase the specific surface area and these structures were conducive to HMs adsorption site(Yang et al. 2022). The BET curves showed that the adsorption/desorption isotherms of CROF were type IV(Fig. 1c), and hysteresis of type H3 was observed, indicating CROF is a porous structure(Li et al. 2021b). The adsorption was minimal when P/P0 between 0 and 0.6 and the isotherm did not achieve the equilibrium when P/P0 was close to 1.0, so there are macropore (> 50 nm) and micropores (2 nm) in CROF(Jiang et al. 2018).It can further concluded that CROF has a BET surface area of 2.5822 m^2/g, a totel pore volume of 0.0083 cm^3/g, and an average diameter of pore was 16.6747 nm. Figure 1(d) showed PSD of CROF presented parabolic distribution, particle size ranged from 23.5 to 117.1 μm, and the median diameter is 36.8 μm. Figure 1(e) showed PH_{PZC} of CROF was 7.02.

3.2 Adsorption process

3.2.1 Adsorption kinetics

Figure 2(a) showed the kinetics of Pb^{2+} adsorption on CROF. 97% of the Pb^{2+} was adsorbed onto the CROF within 20 min, then Pb^{2+} removal rate became slower until the equilibrium states at 60 min as the reaction progress. The large number of surface absorb sites that are available on the CROF and Pb^{2+} concentration decrease may account for the initial rapid adsorption(Wang et al. 2022d; Spessato et al. 2019), and this may be due to the surface electrostatic attraction between Pb^{2+} and OFGs on CROF(Wang et al. 2015).

The parameters derived from PFO, PSO and Elovich kinetic models are presented in Table 1, the R^2 of PFO, PSO and Elovich kinetic models were 0.754, 0.991 and 0.871, respectively.So clearly PSO was the best kinetic models(Wang et al. 2022b) ,this proves that chemical adsorption is more significant than physical adsorption and that the chemisorption phase of Pb^{2+} adsorption on CROF will regulate the pace of adsorption(Wang et al. 2022c).

Table1 Parameters of PFO, PSO, and Elovich models for Pb removal onto CROF

PFO			PSO				Elovich		
K1/ min-1	Qe/mg•g-1	R2	K_2/ g•mg^{-1}•min^{-1}	Q_e/mg•g^{-1}	R^2		α	β	R^2
0.505	12.167	0.754	0.226	12.322	0.991		2.983	4.286	0.873
Langmuir			Freundlich		Sips				
KL	Qm	R2	Kf	1/n	R^2	K_{LF}	a	n	R^2
1.648	15.015	0.943	8.186	0.395	0.831	44.222	3.478	1.424	0.957

3.2.2 Adsorption isotherms

The equilibrium adsorption capacity significantly increased with Pb^{2+} concentrations increased(Fig. 2b). Qm determined from the Langmuir model is 15.02 mg/g, which is comparable to the Qe value.

R^2 of Langmuir model was 0.94 (Table 1), indicating Langmuir model could explaining the process of adsorption(Yang et al. 2022). The R_L range of CROF is 0.108–0.012, indicates that this adsorption occurs under beneficial conditions(Zhang et al. 2022).The Freundlich constant 1/n is 0.395 ,also indicating the adsorption is favorable and the adsorption strength is advantageous across the whole Pb^{2+} concentration range(Lin et al. 2022; Yang et al. 2022). The Sips model is essentially Langmuir model combination with Freundlich model. The Sips model (R^2 = 0.96) showed that the adsorption of Pb^{2+} by the CROF had homogeneous and heterogeneous surface adsorption(Karimi et al. 2019).In a word adsorption of Pb^{2+} by the CROF was homogeneous and also heterogeneous surface adsorption.

3.2.3 Adsorption thermodynamics

Figure 2(c) showed the thermodynamics fitting straight line of Pb^{2+} adsorption on CROF. Table 2 presented the thermodynamics parameters according to Van't Hoff and Gibbs free energy formulas, ΔG^{θ} values increased from − 0.2526 kJ mol^{-1} to − 0.0159 kJ mol^{-1} with the increase of temperature(293K to 308K), indicating that the adsorption capacity of CROF can be more favorable at low temperatures(Rahim et al. 2020). ΔH^{θ}= -50.6338kJ•mol^{-1} demonstrates that the Pb^{2+} adsorption process on CROF is an exothermic adsorption pathway(Rahim et al. 2020). ΔS^{θ}<0 illustrates that the randomization of the system is reduced after Pb^{2+} adsorption and an increase of the temperature would reduce the adsorption capacity(Chen et al. 2021b), so low temperatures was suitable for Pb^{2+} adsorption on CROF.

Table 2 Parameters for adsorption thermodynamics of Pb^{2+} on CROF

T/K	ΔG^{θ}/kJ•mol^{-1}	ΔH^{θ}/kJ•mol^{-1}	ΔS^{θ}/J•(L•mol)$^{-1}$
293	-0.2526	-50.6338	-0.00164
298	-0.2296		
303	-0.0942		
308	-0.0159		

3.3 Adsorption mechanisms

3.3.1 EDS analysis

Figure 3b showed that EDX analyses on the CROF, Pb^{2+} was detected on the surface of CROF after 50mg/ L treated, the content of Pb^{2+} is 1.1 wt %, and Pb^{2+} is homogeneously distributed in the surface of CROF. Meanwhile, other elements such as C, O, Ca, Al have some changes, the Ca percent on CROF was from 3.5 wt % to 2.6 wt % and Al was disappeared after the adsorption process (Fig. 3), confirming the ion exchange between Pb^{2+} and Ca^{2+}onto CROF(Liang et al. 2020).So, CROF could absorb a lot of Pb^{2+},and homogeneously distributed in the surface CROF, adsorption mechanism was the ion exchange between Pb^{2+} and Ca^{2+}.

3.3.2 FTIR analysis

Figure 4 shows the FTIR spectra of CROF under Pb^{2+}. The peak at 3350.06 cm^{-1} could be assigned to the -NH_2 and -OH groups (Wang et al. 2022c), shifted to 3405.94 and 3348.83 cm^{-1} and bacame abviously weaker under 5.0 and 50.0mg/L Pb^{2+}, respectively.This result indicated the binding of Pb^{2+} with O–H and N–H groups(Liang et al. 2020). The peak at 1070 had blueshift also, implying the weak binding of Pb with -N-H (Fang et al. 2022). The -CH and -CH_2 stretching vibration in lignin and polysaccharides was exhibited by the peak at 2923 cm^{-1} (Zong et al. 2020), these heterocyclic compounds promptly bonded to Pb^{2+} as they possessed a weak cation-binder(Yang et al. 2021). While the absorption of C = C groups is located at 1650 cm^{-1}, the peak at 1637.31 cm^{-1} is more notable for carbonyl/carboxyl C = O groups(Wang et al. 2021). Fang et al. (2022) also demonstrated –COOH functional group showed the strong interaction with Pb^{2+}. After treating CROF and Pb^{2+}(5 mg/L), the characteristic peak at 1640.28 cm^{-1} in the control group, moved to 1637.31 cm^{-1}, demonstrating electrostatic attraction or coordination complexation between the lone pairs of electrons on the C = O in CROF and empty orbitals of Pb^{2+}(Tang et al. 2022).but the peak shifted to 1647 cm^{-1} after treating CROF with Pb^{2+}(50 mg/L), remarkably. This phenomenon may be due to the formation of Pb-π interaction(Wang et al. 2021). The stretching of C-O-H and C-O-C peak at 1250 cm^{-1} (Qin et al. 2020;Yang et al. 2020) were blueshift indicating that the C-O of esters and aromatic hydrocarbons could bond with Pb^{2+}.So CROF could bind with Pb^{2+} by Pb-πinteraction and surface complexation between OFGs and NFGs.

3.3.3 XPS analysis

The XPS spectra of CROF and Pb^{2+} was showed in Fig. 5a. Pb4f was appeared in the CROF spectrum when the Pb^{2+} concentrations were 5.0 and 50 mg/L, respectively, indicating that Pb^{2+} was adsorbed by the CROF.

As shown in Fig. 5 (b), two new peaks of Pb4f located at 136.79 and 143.69 eV were appeared when the Pb^{2+} concentration was 5.0 mg/L, Pb4f spectra appeared at 138.81 and 143.71 eV under 50.0 mg/L Pb^{2+} which were ascibed to the Pb^{2+} and O-Pb (Liang et al. 2020).

The C1s, O1s, and N1s of CROF were investigated at Pb^{2+} concentrations of 0, 5.0, and 50 mg/L(Fig. 5.).Four peaks of C = C/C-H bond(284.80 eV)), C-O/C-N bond(286.33 eV), C = O/N-C = O/O-C-O bond(287.9 eV), O-C = O bond(289.49 eV) was appeared (Fig. 5c)(Cai et al. 2021;Ling et al. 2017;Song et al. 2021;Tang et al. 2022). The relative percentage of C-O/C-N decreased from 30.14–26.40% and 27.64%, percentage of C = C/C-H and O-C = O was rose after Pb^{2+} adsorption, and the binding energy was changed, revealed that the the π-π bindings of Pb^{2+} (Wang et al. 2015), and these findings were matched with FTIR analyses.

The O1s spectrum contains the N-C = O(~ 531.4 eV) and C-O-C(~ 532.68 eV)/ C-O-H (~ 533.59 eV) (Fig. 5d)(Liang et al. 2020;Song et al. 2021). The binding energy increased when Pb^{2+} complex to OFGs (De Jong et al. 1994 and Tang et al. 2021). The relative percentage of N-C = O increased from 50.86–56.68% and C-O-C/ C-O-H decreased from 49.14–43.34% when the Pb^{2+}concentration is 5.0 mg/L. When the Pb^{2+} concentration was 50.0 mg/L, the relative proportion of N-C = O declined from 50.86–47.88% whereas the relative proportion of C-O-C/C-O-H climbed from 49.14–52.12%, which may suggest that C-O-C/ C-O-H bind with Pb^{2+} at lower Pb^{2+} concentrations, and N-C = O pays a major role in higher Pb^{2+}concentations

In Fig. 5(d),the N1s assigned to N-C = O and -NH_2 shifted to 401.08 and 400.70 eV (Li et al. 2021b;Song et al. 2021). The Pb^{2+} empty orbital received one pair of electrons from the N atom, which resulted in a lower electron density and a greater binding energy(Zhou et al. 2005). The relative percentage of$\mathrm{NH_3^-}$ decreased and binding energy peak disappeared when Pb^{2+} concentrations were 5.0 mg/L and 50.0 mg/L, which due its transformation into metal complexes(Gao et al. 2017;Wang et al. 2022a).

So the form of Pb in CROF was Pb^{2+} and Pb combined with OFGs(C = O/OH and C-O-C/ C-O-H) and NFGs(N-C = O, -NH_2, $\mathrm{NH_3^-}$)and Pb-πinteraction(C = C).

3.3.4 The simulation process of CROF adsorb Pb^{2+}

Based on the results of the above exploration, we may draw the conclusion that the adsorption mechanisms of Pb^{2+} onto CROF described in Fig. 6.

The process of CROF adsorb Pb^{2+} may be include pore filling, ion exchange, Pb-πinteraction, electrostatic attraction and surface complexation(Wang et al. 2015) between OFGs and NFGs(Fig. 6).Surface complexation with C = O/OH was relatively dominant when the Pb^{2+}concentrations of solution were lower (Pb^{2+} concentration ≤ 5 mg/L),and have a small quantity of electrostatic attraction)(Liang et al. 2020). Pb-πinteraction strengthened and surface complexation between NFGs such as N-C = O, -NH_2, $\mathrm{NH_3^-}$ and C-O-C/ C-O-H in bind with Pb^{2+} at

higher Pb^{2+} concentration(50 mg/L) (Li et al. 2021b;Song et al. 2021). Meanwhile, ion exchange and pore filling of physical action work at both higher and lower Pb^{2+}concentrations.

Conclusions

The CROF has porous structure,the particle size is normally distributed with a median diameter of 36.8 μm, PH_{PZC} of CROF was 7.02.

The Qm of CROF was 15.02 mg/g,and the balance time for the adsorption was 20 minutes. The Pb^{2+} adsorption process of CROF was exothermic, spontaneous and with minimal randomness.

Pb^{2+} mainly binding mechanisms with surface of CROF were pore filling, ion exchange, Pb-πinteraction, and espicially surface complexation of OFGs and NFGs.

Declarations

Ethical Approval

Not applicable.

Consent to Participate

We consent to participate this manuscript.

Consent to Publish

We consent to publish this manuscript.

Authors Contributions

Xiao-yu Feng and Ling-sheng Li have designed experimental scheme, Yu Sun, Xin-yi Tao, Qian Yin, Xin-yue Li and Shi-ying Ma did experiments, De-ju Cao and Zhao-wen Liu have collated and analyzed experimental data, Lu-sheng Zhang mainly responsible for write manuscript.

Funding

This work was under Natural Science Foundation of China (41877418), the financial aid of Nature Fund of Anhui Province of China (1808085MD100) and Funding for this study was provided by Natural Students' Innovation and Entrepreneurship Training Program (X202210364125 X202210364133) also.

Competing Interests

The authors declare that they have no conflict of interest.

Availability of data and materials

We declared that the data and materials presented in this paper are reliable.

References

1. Ahmad M, Zhang B, Wang J, Xu J, Manzoor K, Ahmad S, Ikram S (2019): New method for hydrogel synthesis from diphenylcarbazide chitosan for selective copper removal. International journal of biological macromolecules 136, 189-198. http://doi.org/10.1016/j.ijbiomac.2019.06.084
2. Cai T, Liu X, Zhang J, Tie B, Lei M, Wei X, Peng O, Du H (2021): Silicate-modified oiltea camellia shell-derived biochar: A novel and cost-effective sorbent for cadmium removal. Journal of Cleaner Production 281, 125390. http://doi.org/10.1016/j.jclepro.2020.125390
3. Cao D-j, Shi X-d, Li H, Xie P-p, Zhang H-m, Deng J-w, Liang Y-g (2015): Effects of lead on tolerance, bioaccumulation, and antioxidative defense system of green algae, Cladophora. Ecotoxicology and Environmental Safety 112, 231-237. http://doi.org/10.1016/j.ijbiomac.2019.06.084
4. Chen Q-y, Yang L, Liu L, Qian L-w, Tian K-l, Zhang Q, Cao D-j (2021a): Combined forms of Pb and its detoxification and absorption in Cladophora rupestris subcells. Spectrochimica Acta Part A: Molecular and Biomolecular Spectroscopy 248, 119190. http://doi.org/10.1016/j.saa.2020.119190
5. Chen Y, Tang J, Wang S, Zhang L, Sun W (2021b): Bimetallic coordination polymer for highly selective removal of Pb (II): Activation energy, isosteric heat of adsorption and adsorption mechanism. Chemical Engineering Journal 425, 131474. http://doi.org/10.1016/j.cej.2021.131474
6. De Jong B, Ellerbroek D, Spek A (1994): Low-temperature structure of lithium nesosilicate, Li4SiO4, and its Li1s and O1s X-ray photoelectron spectrum. Acta Crystallographica Section B: Structural Science 50, 511-518. http://doi.org/10.1107/s0108768194002375
7. Esakkimuthu E, DeVallance D, Pylypchuk I, Moreno A, Sipponen M (2022): Multifunctional lignin-poly (lactic acid) biocomposites for packaging applications. Frontiers in bioengineering and biotechnology 10. https://doi.org/10.3389/fbioe.2022.1025076
8. Fang Y, Ren G, Ma Y, Wang C, Li M, Pang X, Pan Q, Li J (2022): Adsorption and reutilization of Pb (II) based on acid-resistant metal-organic gel. Separation and Purification Technology, 121253. http://doi.org/10.1016/j.seppur.2022.121253
9. Gao X, Zhang Y, Zhao Y (2017): Biosorption and reduction of Au (III) to gold nanoparticles by thiourea modified alginate. Carbohydrate Polymers 159, 108-115. http://doi.org/10.1016/j.carbpol.2016.11.095
10. Jayakumar V, Govindaradjane S, Rajamohan N, Rajasimman M (2022): Biosorption potential of brown algae, Sargassum polycystum, for the removal of toxic metals, cadmium and zinc. Environmental Science and Pollution Research 29, 41909-41922. http://doi.org/10.1007/s11356-021-15185-7
11. Jiang B, Lin Y, Mbog JC (2018): Biochar derived from swine manure digestate and applied on the removals of heavy metals and antibiotics. Bioresource Technology 270, 603-611. http://doi.org/10.1016/j.biortech.2018.08.022
12. Jiang Y, Qin Z, Fei J, Ding D, Sun H, Wang J, Yin X (2022): Surfactant-induced adsorption of Pb (II) on the cracked structure of microplastics. Journal of Colloid and Interface Science 621, 91-100. http://doi.org/10.1016/j.jcis.2022.04.068
13. Karimi S, Yaraki MT, Karri RR (2019): A comprehensive review of the adsorption mechanisms and factors influencing the adsorption process from the perspective of bioethanol dehydration. Renewable and Sustainable Energy Reviews 107, 535-553. http://doi.org/10.1016/j.rser.2019.03.025
14. Li J, Zhang Y, Zhou Y, Fang F, Li X (2021a): Tailored metal-organic frameworks facilitate the simultaneously high-efficient sorption of UO22+ and ReO4− in water. Science of The Total Environment 799, 149468. http://doi.org/10.1016/j.scitotenv.2021.149468

15. Li W, Zhang L, Hu D, Yang R, Zhang J, Guan Y, Lv F, Gao H (2021b): A mesoporous nanocellulose/sodium alginate/carboxymethyl-chitosan gel beads for efficient adsorption of Cu2+ and Pb2+. International Journal of Biological Macromolecules 187, 922-930. http://doi.org/10.1016/j.ijbiomac.2021.07.181
16. Liang R-h, Li Y, Huang L, Wang X-d, Hu X-x, Liu C-m, Chen M-s, Chen J (2020): Pb2+ adsorption by ethylenediamine-modified pectins and their adsorption mechanisms. Carbohydrate polymers 234, 115911. http://doi.org/10.1016/j.carbpol.2020.115911
17. Lin X, Shen T, Li M, Shaoyu J, Zhuang W, Li M, Xu H, Zhu C, Ying H, Ouyang P (2022): Synthesis, characterization, and utilization of poly-amino acid-functionalized lignin for efficient and selective removal of lead ion from aqueous solution. Journal of Cleaner Production 347, 131219. http://doi.org/10.1016/j.jclepro.2022.131219
18. Ling L-L, Liu W-J, Zhang S, Jiang H (2017): Magnesium oxide embedded nitrogen self-doped biochar composites: fast and high-efficiency adsorption of heavy metals in an aqueous solution. Environmental Science & Technology 51, 10081-10089. http://doi.org/10.1021/acs.est.7b02382.
19. Qin J, Li Q, Liu Y, Niu A, Lin C (2020): Biochar-driven reduction of As (V) and Cr (VI): Effects of pyrolysis temperature and low-molecular-weight organic acids. Ecotoxicology and environmental safety 201, 110873. http://doi.org/10.1016/j.ecoenv.2020.110873
20. Rahim ARA, Mohsin HM, Thanabalan M, Rabat NE, Saman N, Mat H, Johari K (2020): Effective carbonaceous desiccated coconut waste adsorbent for application of heavy metal uptakes by adsorption: Equilibrium, kinetic and thermodynamics analysis. Biomass and Bioenergy 142, 105805. http://doi.org/10.1016/j.biombioe.2020.105805
21. Song J, Messele SA, Meng L, Huang Z, El-Din MG (2021): Adsorption of metals from oil sands process water (OSPW) under natural pH by sludge-based Biochar/Chitosan composite. Water Research 194, 116930. http://doi.org/10.1016/j.watres.2021.116930
22. Spessato L, Bedin KC, Cazetta AL, Souza IP, Duarte VA, Crespo LH, Silva MC, Pontes RM, Almeida VC (2019): KOH-super activated carbon from biomass waste: Insights into the paracetamol adsorption mechanism and thermal regeneration cycles. Journal of hazardous materials 371, 499-505. http://doi.org/10.1016/j.jhazmat.2019.02.102
23. Sucaldito MR, Camacho DH (2017): Characteristics of unique HBr-hydrolyzed cellulose nanocrystals from freshwater green algae (Cladophora rupestris) and its reinforcement in starch-based film. Carbohydrate Polymers 169, 315-323. https://doi.org/10.1016/j.carbpol.2017.04.031
24. Tang S, Lin L, Wang X, Yu A, Sun X (2021): Interfacial interactions between collected nylon microplastics and three divalent metal ions (Cu (II), Ni (II), Zn (II)) in aqueous solutions. Journal of Hazardous Materials 403, 123548. http://doi.org/10.1016/j.jhazmat.2020.123548
25. Tang S, Yang X, Zhang T, Qin Y, Cao C, Shi H, Zhao Y (2022): Adsorption mechanisms of metal ions (Pb, Cd, Cu) onto polyamide 6 microplastics: New insight into environmental risks in comparison with natural media in different water matrices. Gondwana Research 110, 214-225. http://doi.org/10.1016/j.gr.2022.06.017
26. Wang Q, Wang Y, Yang Z, Han W, Yuan L, Zhang L, Huang X (2022a): Efficient removal of Pb (II) and Cd (II) from aqueous solutions by mango seed biosorbent. Chemical Engineering Journal Advances 11, 100295. http://doi.org/10.1016/j.ceja.2022.100295
27. Wang S, Wang H, Wang S, Zhang L, Fu L (2022b): Highly effective and selective adsorption of Au (III) from aqueous solution by poly (ethylene sulfide) functionalized chitosan: Kinetics, isothermal adsorption and

thermodynamics. Microporous and Mesoporous Materials 341, 112074. http://doi.org/10.1016/j.micromeso.2022.112074

28. Wang X, Jing Y, Cao Y, Xu S, Chen L (2019): Effect of chemical aging of Alternanthera philoxeroides-derived biochar on the adsorption of Pb (II). Water Science and Technology 80, 329-338. http://doi.org/10.2166/wst.2019.276
29. Wang X, Zhang H, He Q, Xing H, Feng K, Guo F, Wang W (2022c): Core-shell alginate beads as green reactor to synthesize grafted composite beads to efficiently boost single/co-adsorption of dyes and Pb (II). International Journal of Biological Macromolecules 206, 10-20. http://doi.org/10.1016/j.ijbiomac.2022.02.091
30. Wang Y, van Zwieten L, Wang H, Wang L, Li R, Qu J, Zhang Y (2022d): Sorption of Pb (II) onto biochar is enhanced through co-sorption of dissolved organic matter. Science of The Total Environment 825, 153686.http://doi.org/10.1016/j.scitotenv.2022.153686
31. Wang Z, Liu G, Zheng H, Li F, Ngo HH, Guo W, Liu C, Chen L, Xing B (2015): Investigating the mechanisms of biochar's removal of lead from solution. Bioresource technology 177, 308-317. http://doi.org/10.1016/j.biortech.2014.11.077
32. Wang Z, Xu J, Yellezuome D, Liu R (2021): Effects of cotton straw-derived biochar under different pyrolysis conditions on Pb (II) adsorption properties in aqueous solutions. Journal of Analytical and Applied Pyrolysis 157, 105214. http://doi.org/10.1016/j.jaap.2021.105214
33. Xu X, Ouyang X-k, Yang L-Y (2021): Adsorption of Pb (II) from aqueous solutions using crosslinked carboxylated chitosan/carboxylated nanocellulose hydrogel beads. Journal of Molecular Liquids 322, 114523. https://doi.org/10.1016/j.molliq.2020.114523
34. Yang G, Zhang N, Yang J, Fu Q, Wang Y, Wang D, Tang L, Xia J, Liu X, Li X (2020): Interaction between perfluorooctanoic acid and aerobic granular sludge. Water research 169, 115249. https://doi.org/10.1016/j.watres.2019.11524
35. Yang X, Chen L, Ren D, Wang S, Ren Z (2022): Adsorption of Pb (II) from water by treatment with an O-hydroxyphenyl thiourea-modified chitosan. International Journal of Biological Macromolecules 220, 280-290. http://doi.org/10.1016/j.ijbiomac.2022.08.090
36. Yang Z, Hou J, Wu J, Miao L (2021): The effect of carbonization temperature on the capacity and mechanisms of Pb (II) adsorption by microalgae residue-derived biochar. Ecotoxicology and Environmental Safety 225, 112750. https://doi.org/10.1016/j.ecoenv.2021.112750
37. Zeng Q, Huang Y, Huang L, Li S, Hu L, Xiong D, Zhong H, He Z (2020): A novel composite of SiO2 decorated with nano ferrous oxalate (SDNF) for efficient and highly selective removal of Pb2+ from aqueous solutions. Journal of hazardous materials 391, 122193. http://doi.org/10.1016/j.jhazmat.2020.122193
38. Zhang H-m, Geng G, Wang J-j, Xin Y, Zhang Q, Cao D-j, Ma Y-h (2019): The remediation potential and kinetics of cadmium in the green alga Cladophora rupestris. Environmental Science and Pollution Research 26, 775-783. http://doi.org/10.1007/s11356-018-3661-z
39. Zhang S, Arkin K, Zheng Y, Ma J, Bei Y, Liu D, Shang Q (2022): Preparation of a composite material based on self-assembly of biomass carbon dots and sodium alginate hydrogel and its green, efficient and visual adsorption performance for Pb2+. Journal of Environmental Chemical Engineering 10, 106921. http://doi.org/10.1016/j.jece.2021.106921

40. Zhang Y, Wang Y, Zhang X, Li R, Chen Y, Meng Q (2017): Investigating the behavior of binding properties between dissolved organic matter (DOM) and Pb (II) during the soil sorption process using parallel factor analysis (PARAFAC) and two-dimensional correlation spectroscopy (2D-COS). Environmental Science and Pollution Research 24, 25156-25165. http://doi.or/z10.1007/s11356-017-0167-z
41. Zhou D, Zhang L, Guo S (2005): Mechanisms of lead biosorption on cellulose/chitin beads. Water Research 39, 3755-3762. http://doi.org/10.1016/j.watres.2005.06.033
42. Zong P, Jiang Y, Tian Y, Li J, Yuan M, Ji Y, Chen M, Li D, Qiao Y (2020): Pyrolysis behavior and product distributions of biomass six group components: Starch, cellulose, hemicellulose, lignin, protein and oil. Energy Conversion and Management 216, 112777. http://doi.org/10.1016/j.enconman.2020.112777

Figures

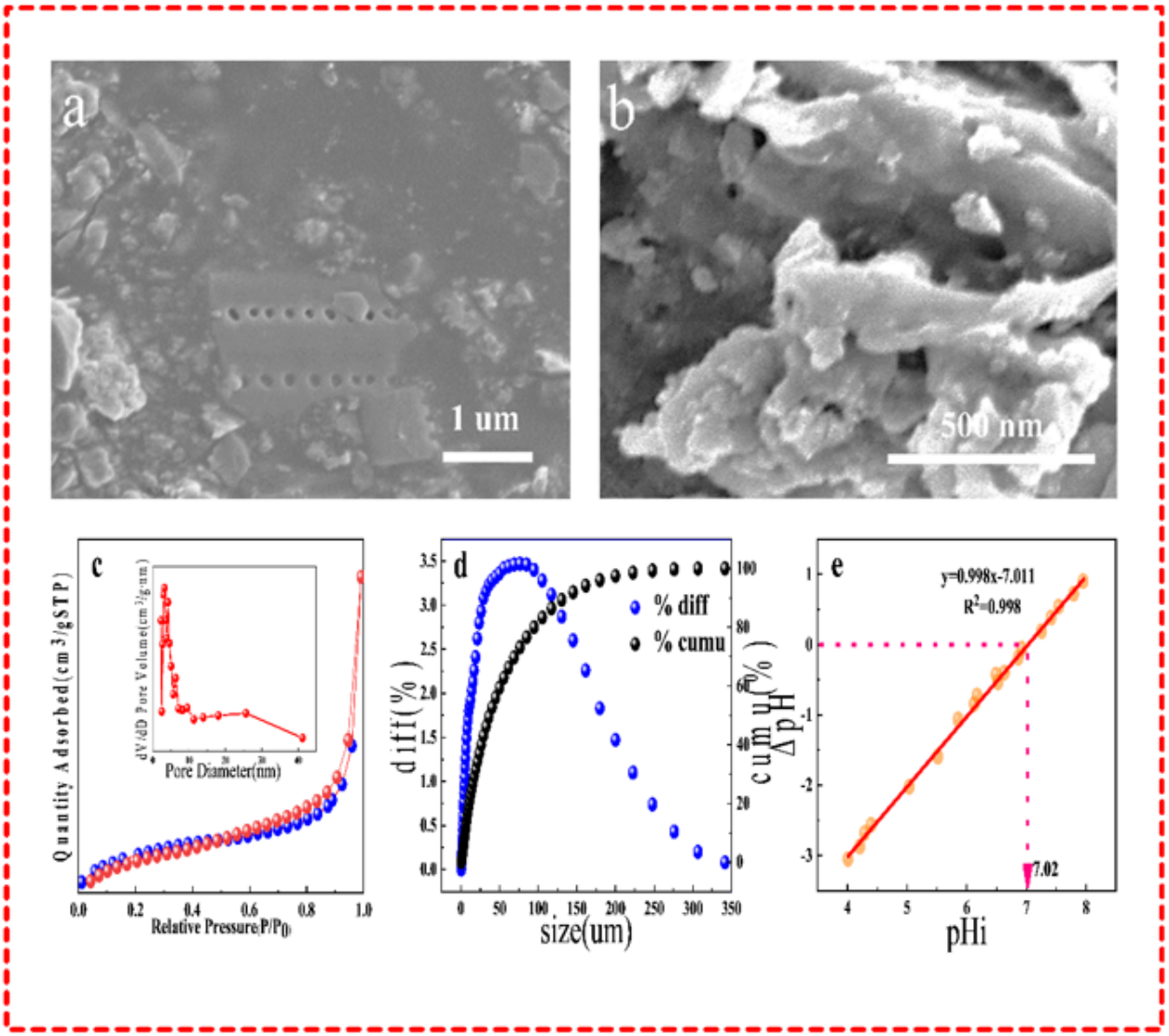

Figure 1

SEM images (a,b), PSD(c), BET(d), PH_{PZC}(e) of CROF

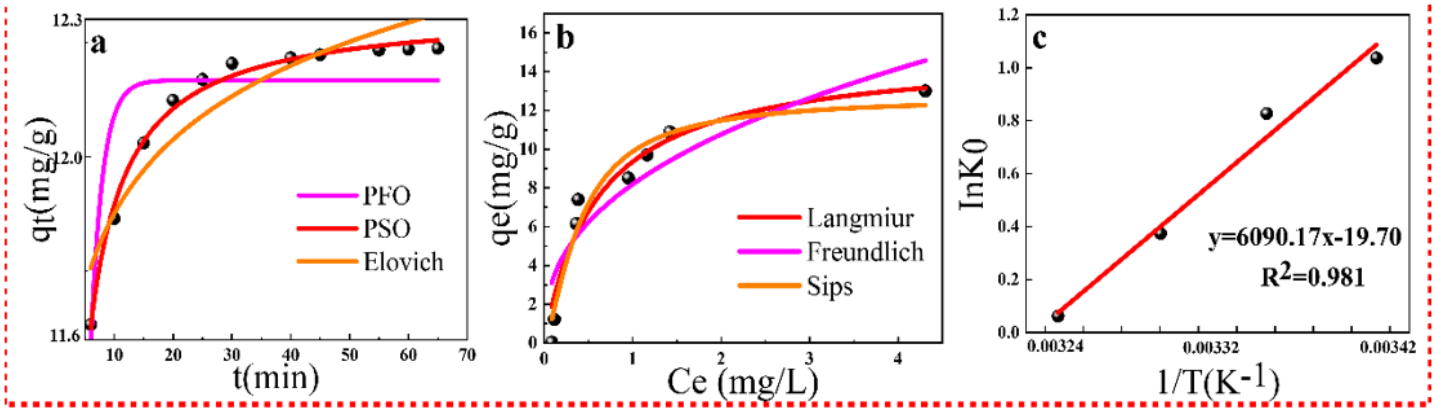

Figure 2

Adsorption kinetics(b), adsorption isotherms(a) and adsorption thermodynamics of Pb^{2+} sorption on CROF

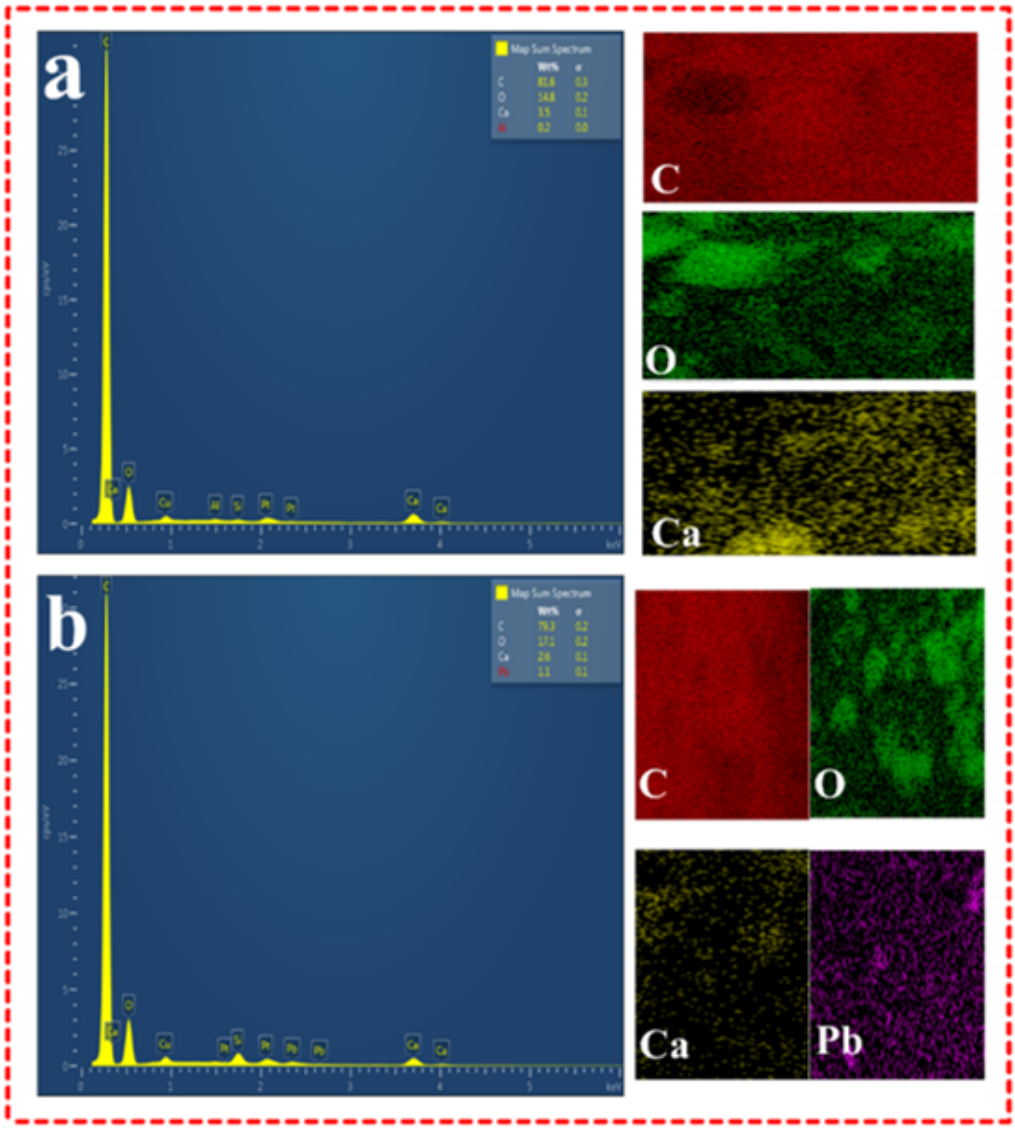

Figure 3

EDS spectrum of CROF before(a) and after(b) treated with Pb^{2+}

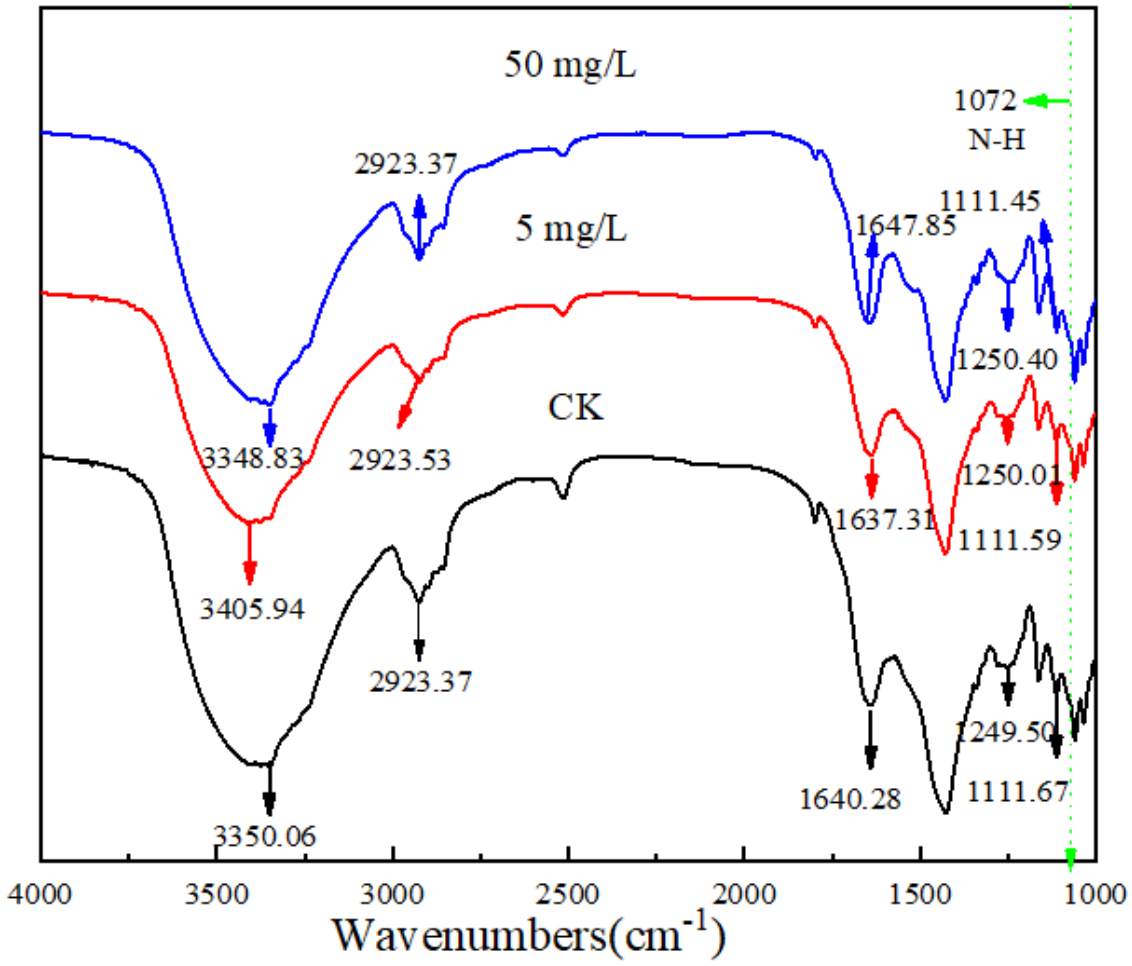

Figure 4

The FTIR pectra of CROF before and after adsorption Pb^{2+}

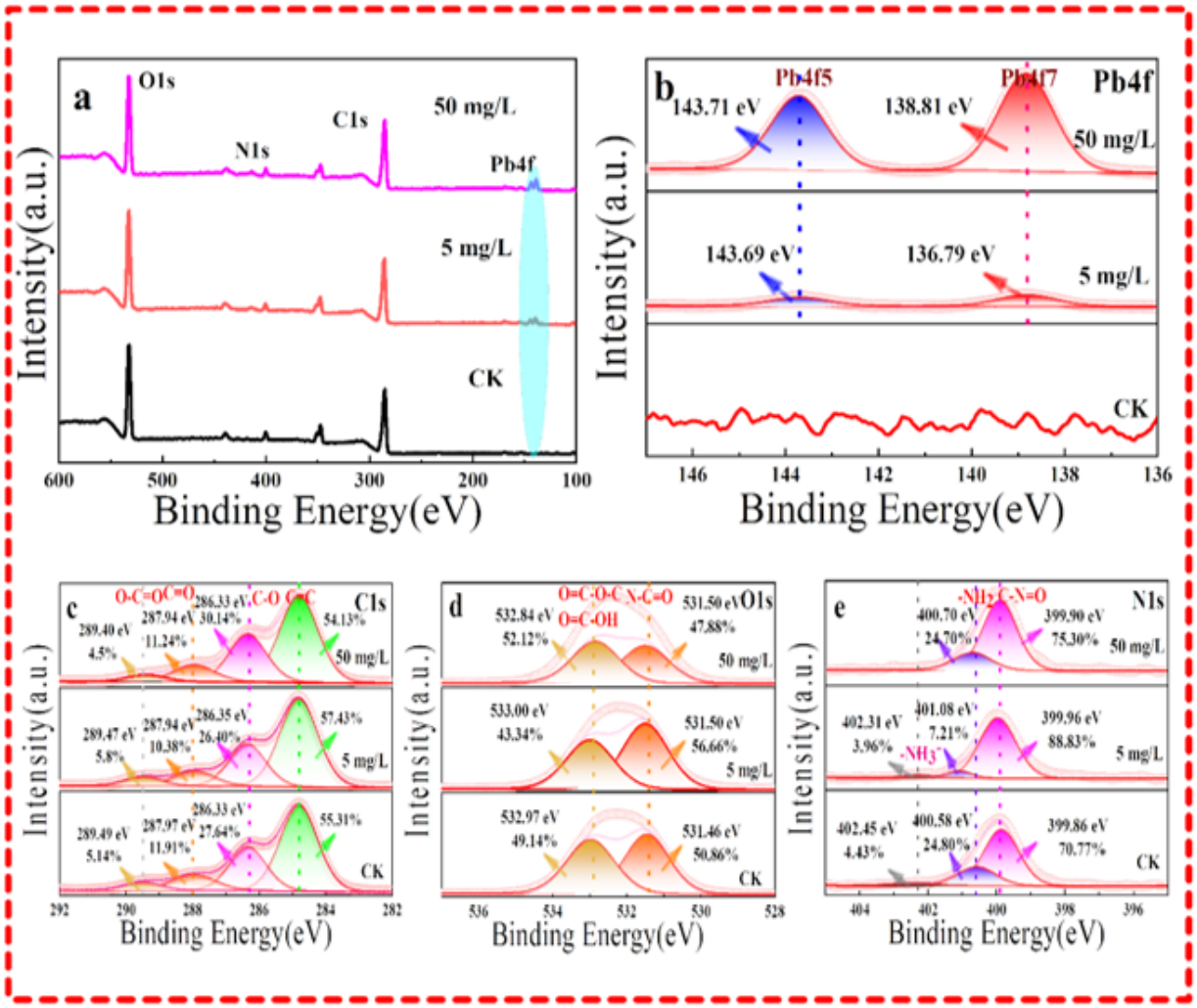

Figure 5

Pb4f spectra(a),C1s spectra(b),O1s spectra (c), and N1s spectra(d) of CROF before and after adsorption Pb^{2+}

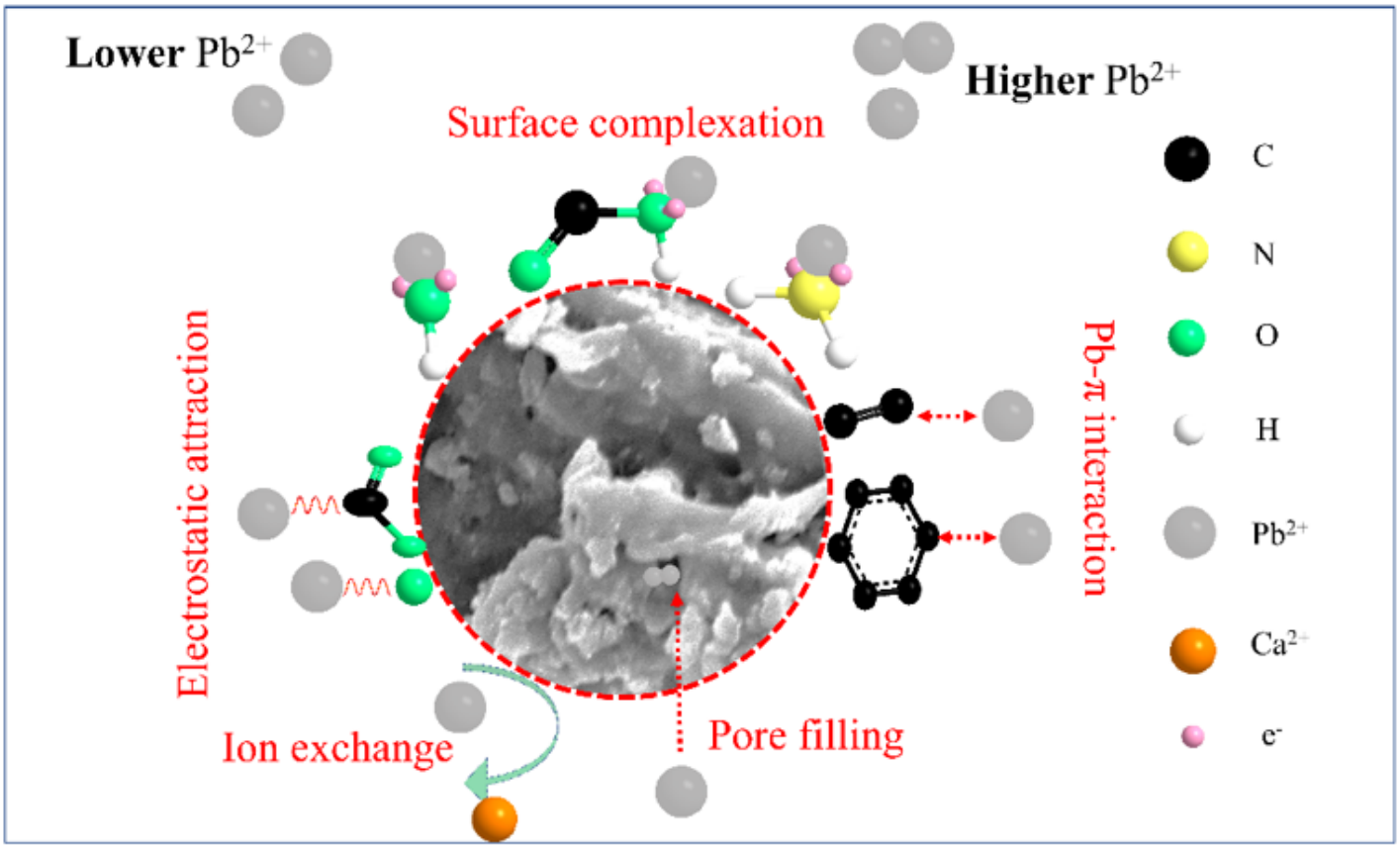

Figure 6

The simulation process of CROF adsorb Pb^{2+}